



# Probing ionization characteristics of under-water plasma arc discharge using simultaneous current and voltage versus time measurement in carbon nanoparticle synthesis

Miftahul Anwar<sup>a,\*</sup>, Teguh E. Saraswati<sup>b</sup>, Lia Anjarwati<sup>a</sup>, Daniel Moraru<sup>c</sup>, Arief Udharto<sup>d</sup>, Feri Adriyanto<sup>a</sup>, Hari Maghfiroh<sup>a</sup>, Ratno Nuryadi<sup>e,f</sup>

<sup>a</sup> Department of Electrical Engineering, Faculty of Engineering, Sebelas Maret University, Surakarta 57126, Indonesia

<sup>b</sup> Department of Chemistry, Faculty of Mathematics and Natural Sciences, Sebelas Maret University, Surakarta 57126, Indonesia

<sup>c</sup> Research Institute of Electronics, Shizuoka University, Hamamatsu 432-8011, Japan

<sup>d</sup> Department of Electrical Engineering, Faculty of Engineering, Universitas Indonesia, Depok 16424, Indonesia

<sup>e</sup> Center for Materials Technology, Agency for the Assessment and Application of Technology, Puspiptek Building #224, South Tangerang, Banten 15314, Indonesia

<sup>f</sup> Sinar Cendekia College of Education, Serpong, South Tangerang, Banten 15310, Indonesia



## ARTICLE INFO

### Keywords:

Ionization characteristics  
I-t and V-t measurement  
Probing  
Underwater arc discharge  
Plasma diagnostics

## ABSTRACT

This study investigated the characteristics of plasma ionization that occurs during plasma arc discharge in water using carbon electrodes. The characterization of plasma ionization begins by observing the arc shape using a digital camera associated with voltage oscillation using current and voltage vs. time (I-t and V-t) characteristics. Furthermore, the ionization energy calculation is performed using simultaneous I-t and V-t measurement data. These calculations are then compared to the photon energy from the optical emission spectroscopy (OES). The results from the digital camera indicate four types of arc discharge in terms of shape and intensity related to voltage oscillation. Moreover, the energy calculations show that by using the I-t and V-t methods is possible to measure the plasma ionization detected not only in the range 1–4 eV but also in the outside range, including smaller than 1 eV and greater than 4 eV. These ranges correspond to the emission lines in visible light, infrared, and ultraviolet, respectively. In addition, the I-t and V-t methods can also measure the excitation and recombination energy of the arc discharge plasma ionization. This study reveals the possibility of investigating the characteristics of plasma ionization using simultaneous I-t and V-t measurements, which comprise an easier and more practical method in the diagnostics of carbon nanoparticle synthesis

## 1. Introduction

Over the past decade, plasma diagnostics has been a topic of interest for researchers studying the characteristics of plasma species in various fields, such as electronics [1], materials synthesis [2], energy [3], and even medicine [4]. One of the plasma applications in materials synthesis, carbon nanomaterial fabrication is a key plasma application. The most common plasma methods for synthesizing carbon nanomaterials are laser ablation [5,6], chemical vapor deposition (CVD) [7,8], and arc discharge [9]. The arc discharge method has some benefits making it preferable to other methods, including fewer defects and high flexibility.

During the arc discharge process, electrons are discharged from the cathode to the anode, causing energy to be released in the gap between

two electrodes. The energy is released in the form of plasma arc discharge at high temperatures, resulting in electrode surface erosion and the formation of carbon nanoparticles [10]. Carbon nanotubes (CNTs) and carbon nano-onions are typical examples of nanoparticles grown in vacuum arc discharge [11] and underwater-submerged arc discharge [12], respectively.

From a technical point of view, many different methods, such as spectroscopy (visible, UV, X-ray), probing, magnetics, laser-aided diagnostics, particle diagnostics, and fusion product diagnostics, have been employed to measure the spatial profile and evolution of various plasma parameters. Such parameters include the following: atomic (ionic) processes; electron temperatures; plasma currents; plasma position, shape, and instability; excited states of specific ion species; energy

\* Corresponding author.

E-mail address: [miftahwar@ft.uns.ac.id](mailto:miftahwar@ft.uns.ac.id) (M. Anwar).

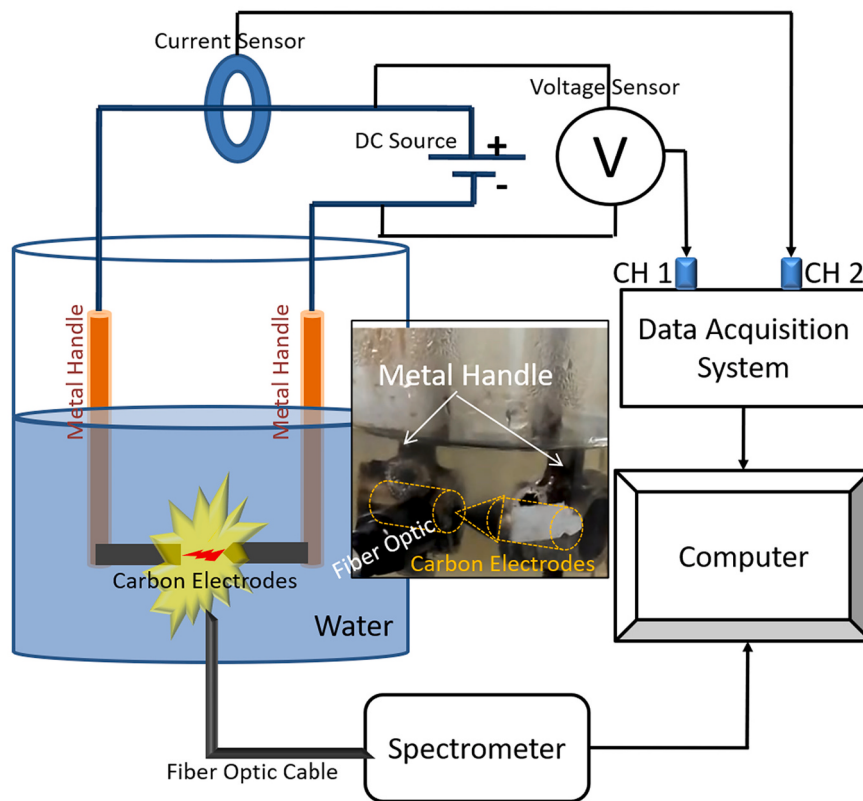


**Fig. 1.** A schematic of the experimental setup consisting of a water-filled chamber, carbon electrodes, a current sensor, voltage sensors, a data acquisition system, a spectrometer, and a computer.

spectrums of neutral particles escaping from plasma; and fusion reactions of specific atoms or particles [13]. Although most of these techniques are well established, plasma diagnostics remains a challenging and vivid discipline in which researchers are constantly striving for ways to perform measurements with greater accuracy.

Diagnostics for plasma arc discharge generally use optical emission spectroscopy (OES), which detects ionized emission species [14]. However, the Langmuir probe can also be used to determine the density of ions that occur, as well as plasma and electron temperatures (in energy) [15]. Thus far, some researchers have applied simultaneous current and voltage vs. time (I-t and V-t) data from the arc discharge to determine the current and voltage conditions when plasma ionization occurs [16–18], including investigating pressure wave propagation characteristics [19] and bubble expansion in water [20]. Nevertheless, the utilization of simultaneous I-t and V-t measurements as a probing method for the ionization energy of plasma arc discharge, which is crucial for understanding the arc shapes and ionization processes of plasma, has never been achieved.

We recently explored the effect of current source variation on the growth of carbon nanoparticles in the underwater-submerged arc discharge [21] and on the energy needed during the first peak of the current [22]. In this paper, for the diagnostics of carbon nanoparticle synthesis, the ionization characteristics of the arc discharge phenomenon underwater using simultaneous I-t and V-t measurements are discussed. Changes in current, voltage, and photographic data on arc shapes during arc discharge are also investigated. Afterward, a numerical analysis of single discharge energy is calculated from the I-t and V-t measurement results to obtain the plasma arc discharge parameters i.e., ionic excitation and recombination process. In addition, this I-t and V-t measurement is compared to the OES data to carry out the ionization energy of plasma arc discharge.

## 2. Measurements and setup

The experiments were conducted using a carbon arc setup, as shown in Fig. 1. This setup consisted of two graphite (99%) electrodes, with a diameter of 1 cm, connected to metal handles, which were dipped in de-ionized water (~30 cm from the surface) with a resistance of ~1 MΩ. The negative electrode (cathode) was deliberately formed with a conical-shaped tip so that the discharged electrons were concentrated at one point. As expected, the potential energy led to an increase in the erosion of and the gap between the electrodes [23] resulting carbon nanoparticles. At that point, a discharge current (i.e., the current between two electrodes) of 40 A was maintained. A current ranging from 30 to 50A is known to be an effective value for growing nano-onions [24]. Depending on the electrodes gap and the anode diameter, the discharge voltage is in the range of 0–30 V. This voltage includes the voltage drop across the electrodes. In the present study, the arc was operated in de-ionized water at atmospheric pressure.

The arc was initiated when the electrodes came close to each other by manually moving the cathode. The distance between the electrodes was kept constant (at around 0.4 mm [20]) as long as the arc discharge continues until it stops naturally due to erosion at the anode to be nanoparticles. To minimize the effect of water flow caused by electrode movement, a mechanical gear was connected to the electrode handle to smoothly move the electrode forward and backward. Next, the current was controlled by maintaining the external DC current source. During arc operation, carbon nanoparticles were formed, which were then collected by filtering. The remaining water was removed using a heater at 200 °C and separated via centrifugation at 4000 rpm (5 min). The dried carbon deposit was further characterized using scanning electron microscopy (SEM, FEI ISPECT-S50, acceleration voltage of 25 kV) and transmission electron microscopy (TEM, JEOL JEM-1400, an accelerating voltage of 120 kV).

The applied voltage was measured using a 1:100 differential probe

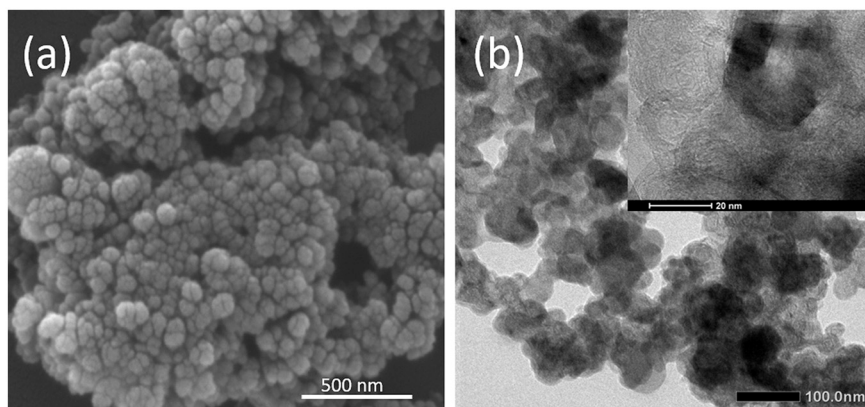


**Fig. 2.** (a) SEM and (b) TEM images of carbon nanoparticles. (b) TEM observation confirms the carbon onion structures, which consist of many layers.

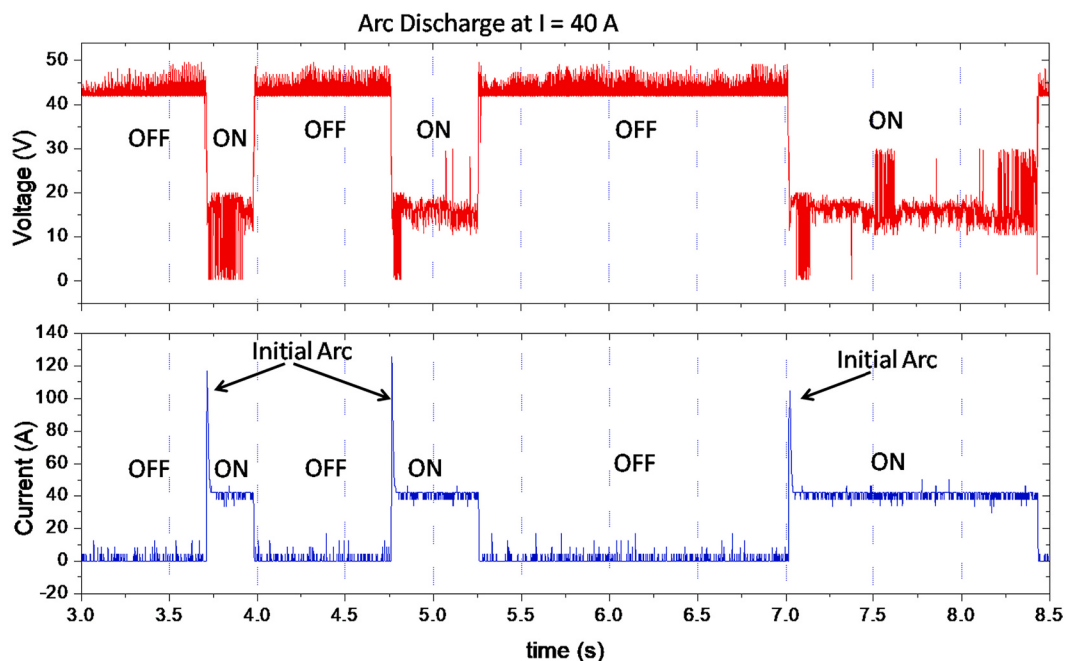


**Fig. 3.** I-t and V-t characteristics of arc discharge. ON/OFF states on I-t (bottom) and V-t (top) graphs indicate that arc discharge appears/disappears sequentially. The anode-cathode distance is  $\sim 0.4$  mm.

(ISDS205) voltage sensor that was connected in parallel to the electrode gap. The current measurements were carried out using the WCS1500 Hall effect current sensor. The voltage and current values were connected to CH1 and CH2 of the data acquisition system, respectively, and then presented in real time to the order of milliseconds. Moreover, OES measurement was also performed to investigate the arc emission characteristics. The spectra were measured using an Ocean Optics Maya 2000 spectrophotometer with an exposure of 1 ms and a repetition rate of 1000 Hz. To investigate the condition when plasma occurred, a digital camera with a speed of 30 frames/s was utilized. With this camera, we were able to record plasma arc states (size and shape). In order to obtain the energy parameter of arc discharge plasma i.e., ionic excitation and recombination process, the energy calculation was then performed to compare single discharge energy, derived from I-t and V-t data, and single photon energy taken from OES data.

### 3. Results and discussion

Carbon powder produced by arc discharge was characterized using SEM and TEM, as shown in Fig. 2(a) and (b), respectively. The carbon

nanoparticles observed in the SEM image had a spherical shape with a diameter of 10–50 nm. Using TEM, the structures of the carbon nanoparticles were confirmed to be carbon onions—i.e., spherical carbon nanoparticles consisting of many layers, as shown in the inset of Fig. 2(b).

The current and voltage versus time characteristics of submerged arc discharge were measured at a steady current of 40 A in real time, as shown in Fig. 3. The ON-state in current and voltage characteristics indicated the existence of arc discharge events, while the OFF-state indicated no arc events ( $I = 0$  A;  $V = \sim 42$  V) during measurement. The initial current of the ON-state was always high (more than 100 A), which indicated that the number of charges flowing between electrodes reached a maximum level due to the high capacitance value that occurred between the two electrodes. According to our recent study [22], when the electrodes were close enough ( $\sim 0.4$  mm), the potential energy was able to break down the dielectric of water, and the arc was naturally initiated. On the other hand, the current value was in a steady state (40 A) when the arc events were maintained. However, at this point, the voltage level fluctuated (0 to 30 V), which was likely due to plasma ionization between the two electrodes. During the 5.5 s range of

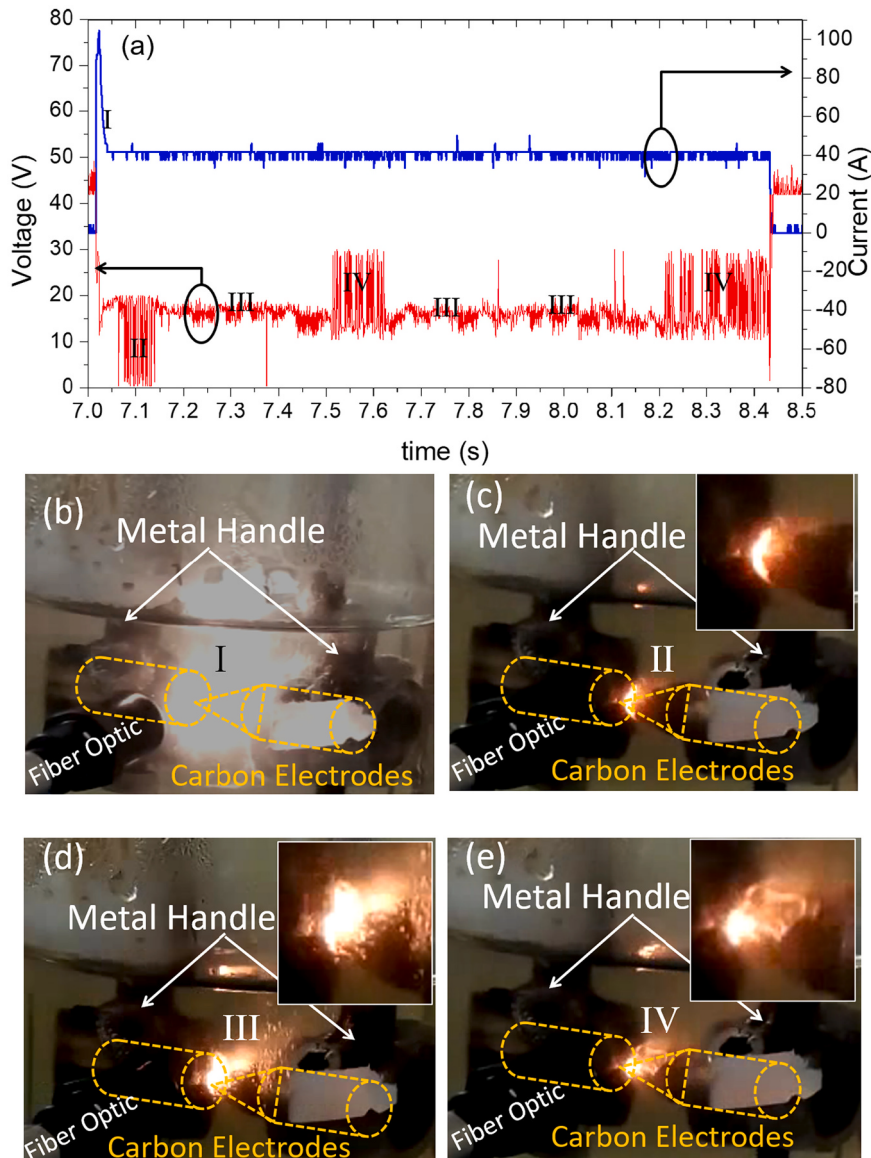


**Fig. 4.** (a) I-t and V-t characteristics at 7 to 8.5 s, which show current and voltage oscillation of states I, II, III, and IV, and (b–e) corresponding photographs of the arc event underwater for each state. The anode-cathode distance is  $\sim 0.4$  mm.

measurement, three initiated arc discharges occurred. A longer time range of arc discharge data is also shown in the supplementary data of Fig. S1.

To understand the ionization characteristics of plasma at arc discharge, an enlarged image of the I-t and V-t of Fig. 3 at 7–8.5 s is shown in Fig. 4(a). In the current graph, after the first peak (state I), the current was stable at 40 A. On the other hand, the voltage graph shows a significant change in the range of 7.05 to 8.45 s before the arc disappeared or turned OFF. Regarding the voltage characteristic in the voltage graph, there were three states (except for the initial peak at the beginning of the ON-state)—i.e., state II, state III, and state IV. State II was a state in which the voltage oscillated at a value of 0 to 20 V. In state III, the voltage was stable at approximately 20 V. However, in state IV, the voltage returned to oscillating at a value between 12 and 30 V, while the current was still maintained at 40 A. Supplementary data shown in Fig. S2 also indicates the same characteristics for a longer discharge time range (5 s range).

Fig. 4(b–e) show photographs of the arc discharge in states I, II, III, and IV, which explain the arc state in real time. In state I (in Fig. 4(a)), the measured current had the highest value correlated to the arc

condition, which is shown in Fig. 4(b). This has a broad arc shape, resulting in the brightest light illumination. In states II, III, and IV, as shown in Fig. 4(c–e), the light illumination produced by the arc weakened with a smaller arc shape. Such differences in arc shape are possible because arch shapes vary with different plasma ionization characteristics of arc discharge.

In Fig. 4(c), which correlates with state II in Fig. 4(a), the voltage is shown oscillating from 0 V to  $\sim 20$  V, indicating that the electrodes in this state were frequently connected (short circuit), thereby producing a drop in voltage oscillation. Thus, the represented arc light illumination was the dimmest compared to the others (see the magnified image in Fig. 4(c)). However, the arc light illumination of states III and IV, as shown in Fig. 4(d) and (e), respectively, were brighter than that of state II. Moreover, the arc shape had a typical irregular form of ionized arc plasma [25–27], as shown in the enlarged image. According to the current continuity at the cathode, the arc current was a combination of electron current and ion current [28,29], as indicated in Eq. (1).

$$I_{arc} = I_{electrons} + I_{ions} \quad (1)$$

Therefore, it is understandable that state I had the high-density arc

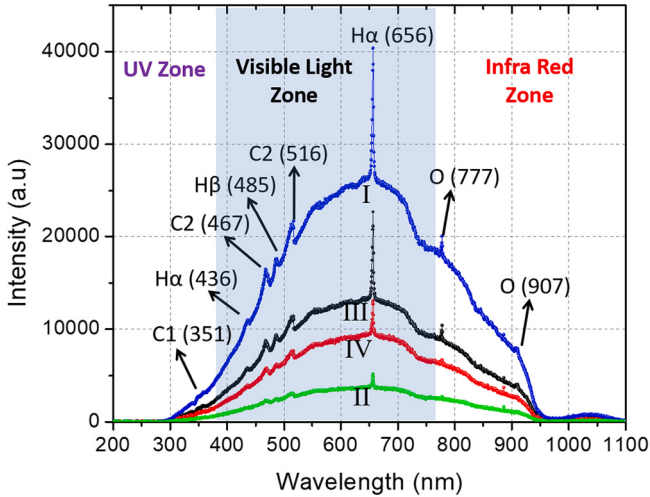


**Fig. 5.** OES spectra of light-emitted arc for different intensities correspond to state I through state IV in I-t and V-t measurements.

current  $I_{arc}$  (for constant electrode area) due to the high potential energy dissipation of a capacitor between the two electrodes with the maximum charge density. State II mainly consisted of the electron current  $I_{electrons}$ , which was indicated by the oscillation of the voltage drop, while state III was a mixture of  $I_{ions}$  and  $I_{electrons}$  (low density of  $I_{arc}$ ), with a small average oscillation of the voltage profile. State IV, in contrast, primarily consisted of ion current  $I_{ions}$ , as indicated by voltage oscillations from approximately 12 to 30 V. Oscillation to a higher voltage (to 30 V) showed that the electrons that flowed from the anode were suppressed by the potential of the excitation and recombination events of plasma ions that occurred between the two electrodes.

Moreover, the intensity and wavelength values of light produced by plasma arc discharge have also been measured using OES, as shown in Fig. 5. Variations in light intensity at areas I, II, III, and IV in Fig. 5 are in accordance with the photographic data shown in Fig. 4(b–e), respectively, which also corresponds to a different state as shown in Fig. 4(a). In general, the wavelength peaks observed in the OES data had the same pattern for all intensity variations. The emission peaks observed at wavelengths 351, 467, and 516 nm represented the emission of C ions vaporized from the electrodes. Furthermore, the peaks of 436, 486, and 636 nm were the emission of H ions, and the peaks of 777 nm and 907

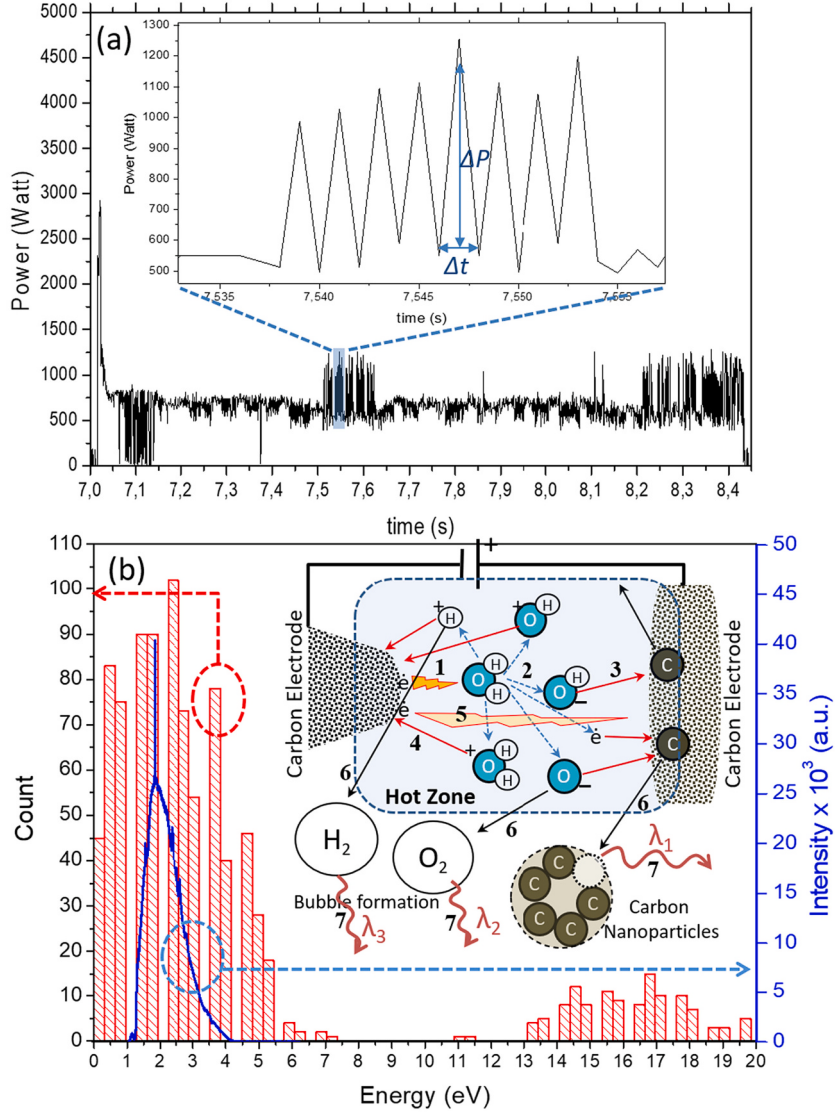


**Fig. 6.** (a) The power graph of the result of multiplying  $V$  and  $I$  vs. time data with the inset graph of the power oscillation with the area  $\Delta P$  (height of the peak) and  $\Delta t$  (time resolution for one peak) as energy for one discharge event. (b) Derived energy from I-t and V-t measurement  $E_1$  (bar chart) and photon energy  $E_2$  from OES with the illustration of charge elementary reaction mechanisms for the formation of nanoparticles and air bubbles in the inset.

nm were the emission of oxygen (O) ions [30].

For further analysis, the energy  $E_1$  was calculated from the data of I-t and V-t of Fig. 4(a), which was compared to the energy  $E_2$  from the OES data in Fig. 5. To calculate  $E_1$  and  $E_2$ , Eqs. (2) and (3) were employed. Fig. 6 shows the results of the power vs. time (Fig. 6(a)) and the energy comparison (Fig. 6(b)) between the single discharge energy  $E_1$  from Eq. (2) (bar chart) and the photon energy  $E_2$  from Eq. (3).

$$E_1 = \frac{E_{disc}}{N} = \frac{\int P(t) dt}{N} \quad (2)$$

$$E_2 = \frac{hc}{\lambda} \quad (3)$$

Where  $E_1$  is the energy of a single discharge event of the arc plasma, and  $E_{disc}$  corresponds to the discharge energy or area of power oscillation changes with time caused by the discharge current.  $P(t)$  is the power obtained by multiplying  $V(t)$  and  $I(t)$  (Fig. 6(a)),  $dt$  is the time range of one peak (see inset of Fig. 6(a)) and  $N$  is the number of charges obtained from current  $I(t)$  data in Fig. 4(a), which is derived from  $N = \frac{\int I(t) dt}{e}$ ;  $e$  is the charge of electron  $1.6 \times 10^{-19} C$ . On the other hand,  $E_2$  in Eq. (3) corresponds to the photon energy detected by OES, where  $h$ ,  $c$ , and  $\lambda$  are the Planck constant ( $6.62607004 \times 10^{-34} m^2 \cdot kg/s$ ), speed of light ( $3 \times 10^8 m/s$ ), and electromagnetic wavelength in nm (obtained from OES data in Fig. 5), respectively.

As shown in Fig. 6(b), the results showed similar features between  $E_1$  (bar chart) and  $E_2$  (line spectra) at approximately 1–4 eV, which corresponds to the energy of visible light (at  $\lambda \approx 400$ –750 nm shown in Fig. 4). However, significant differences in energy  $E_1$  data—i.e., peak appearance at a smaller energy value (< 1 eV) and a larger energy value (> 4 eV) were observed. This result was similar to the result obtained and shown in Fig. S3 (supplementary graph).

The charge elementary reaction mechanism in the arc discharge system is explained in more detail in the inset of Fig. 6(b). Initially, the electrons leave the anode and hit the water molecules (1) when external DC voltage was applied. Water molecules that are hit by electrons are then excited (taken from the electron's kinetic energy) by releasing one of its charges (negative or positive charge) and transforming into several ionic forms (dashed blue arrows) (2). Negative ions and electrons move toward the anode (3), while positive ions move toward the cathode (4) due to the direction of the electric field between the two electrodes, indicated by the low-density  $I_{arcs}$  of state III (Fig. 4). The discharged electrons from the cathode may also go directly to the anode (5) in short circuit events, emphasizing the explanation of voltage drop oscillation in state II in Fig. 4. Moreover, some ions (such as carbon ions released from the anode, H ions, and O ions) move out of the hot zone [21] and form carbon nanoparticles and air bubbles (6), which causes voltage oscillation in state IV (Fig. 4(a)). The formation of nanoparticles and bubbles release energy in the form of light with different wavelengths (7), as detected in OES shown in Fig. 5.

The fundamental difference between the two methods, including I-t and V-t measurement and OES, is that the I-t and V-t measurement methods can measure not only excitation but also the recombination energy due to nanoparticle and bubble formation, which is indicated by voltage oscillation at state IV (in Fig. 4(a)). Therefore, it can be understood that the results of the I-t and V-t energy  $E_1$  can be defined as the energy required by the arc discharge system to carry out the ionization process and carbon nanoparticle formation. On the other hand, the OES method measures only the emission energy of the ion recombination process during nanoparticle and bubble formation, typically in the range 200–1100 nm for a common spectrophotometer. The energy in the lower area beyond visible light (infrared areas) is most likely energy that is transferred to the water and electrodes in the form of phonon energy (heat). Conversely, the phenomenon with energy higher than 4 eV is detectable by I-t and V-t measurements corresponding to the higher voltage oscillation (states II and IV) shown in Fig. 4(a), which is highly

possible coming from the higher excitation energy of arc plasma ionization.

#### 4. Conclusion

Simultaneous I-t and V-t measurement methods have been demonstrated to be effective methods for observing the characteristics of plasma arc discharge for diagnostics of nanoparticle synthesis. The results of this I-t and V-t measurement proved to be accurate as a probing method for the ionization of plasma arc discharge that can amplify OES measurements, which are limited to visible light measurements. These results show that I-t and V-t measurements can measure the ionization of plasma in a wide range, from smaller energy values (infrared wavelength) to higher energy values (ultraviolet wavelength), which opens up new possibilities of plasma diagnostics for understanding both fundamental plasma sciences and applications.

#### Declaration of Competing Interest

The authors declare that they have no known competing financial interests or personal relationships that could have appeared to influence the work reported in this paper.

#### Acknowledgment

We thank Y. Mahardhika and R. Fadhilah for their support in the experiment and discussions. All authors contributed to analyzing the results and reviewing the manuscript. This work was partially supported by Grants-in-Aid for International Collaboration (No: 452/UN27.21/PN/2020), (No: 260/UN27.22/HK.07.00/2021) from Sebelas Maret University, and Grants-in-Aid (Hibah PPI Q1 No: NKB-601/UN2.RST/HKP.05.00/2021) from University of Indonesia.

#### Appendix A. Supplementary data

Supplementary data to this article can be found online at <https://doi.org/10.1016/j.mne.2021.100099>.

#### References

- [1] J.P. Boeuf, Plasma display panels: physics, recent developments and key issues, *J. Phys. D. Appl. Phys.* 36 (6) (2003) R53–R79, <https://doi.org/10.1088/0022-3727/36/6/201>.
- [2] P.R. Taylor, S.A. Pirzada, Thermal plasma processing of materials: a review, *Adv. Perform. Mater.* 1 (1) (1994) 35–50, <https://doi.org/10.1007/BF00705312>.
- [3] Q. Wang, X. Wang, Z. Chai, W. Hu, Low-temperature plasma synthesis of carbon nanotubes and graphene based materials and their fuel cell applications, *Chem. Soc. Rev.* 42 (23) (2013) 8821–8834, <https://doi.org/10.1039/C3CS60205B>.
- [4] G. Morfill, M.G. Kong, J. Zimmermann, Focus on plasma medicine, *New J. Phys.* 11 (11) (2009), 115011.
- [5] S.-K. Chang-Jian, J.-R. Ho, J.W. John Cheng, Fabrication of transparent double-walled carbon nanotubes flexible matrix touch panel by laser ablation technique, *Opt. Laser Technol.* 43 (8) (2011) 1371–1376, <https://doi.org/10.1016/j.optlastec.2011.03.027>.
- [6] Y. Zhang, H. Gu, S. Iijima, Single-wall carbon nanotubes synthesized by laser ablation in a nitrogen atmosphere, *Appl. Phys. Lett.* 73 (26) (1998) 3827–3829, <https://doi.org/10.1063/1.122907>.
- [7] M. Kumar, Y. Ando, Chemical vapor deposition of carbon nanotubes: a review on growth mechanism and mass production, *J. Nanosci. Nanotechnol.* 10 (6) (2010) 3739–3758.
- [8] W. Xia, D. Su, A. Birkner, L. Ruppel, Y. Wang, C. Wöll, J. Qian, C. Liang, G. Marginean, W. Brandl, M. Muhler, Chemical vapor deposition and synthesis on carbon nanofibers: sintering of ferrocene-derived supported iron nanoparticles and the catalytic growth of secondary carbon nanofibers, *Chem. Mater.* 17 (23) (2005) 5737–5742, <https://doi.org/10.1021/cm051623k>.
- [9] G. Xing, S.-L. Jia, Z.-Q. Shi, The production of carbon nanomaterials by arc discharge under water or liquid nitrogen, *New Carbon Mater.* 22 (4) (2007) 337–341, [https://doi.org/10.1016/S1872-5805\(08\)60005-0](https://doi.org/10.1016/S1872-5805(08)60005-0).
- [10] D.A. Mylnikov, A.A. Efimov, V.V. Ivanov, Investigation of the energy balance in the spark discharge generator for nanoparticles synthesis, *J. Phys. Conf. Ser.* 830 (2017), 012162, <https://doi.org/10.1088/1742-6596/830/1/012162>.
- [11] S. Iijima, Helical microtubules of graphitic carbon, *Nature* 354 (6348) (1991) 56–58.

- [12] N. Sano, H. Wang, M. Chhowalla, I. Alexandrou, G.A.J. Amaralunga, Synthesis of carbon'onions' in water, *Nature* 414 (6863) (2001) 506, <https://doi.org/10.1038/35107141>.
- [13] A.J.H. Donné, Introduction to plasma diagnostics, *Fusion Sci. Technol.* 49 (2T) (2006) 349–356, <https://doi.org/10.13182/FST06-A1134>.
- [14] J.W. Coburn, M. Chen, Optical emission spectroscopy of reactive plasmas: a method for correlating emission intensities to reactive particle density, *J. Appl. Phys.* 51 (6) (1980) 3134–3136, <https://doi.org/10.1063/1.328060>.
- [15] G. Thakur, R. Khanal, B. Narayan, Characterization of arc plasma by movable single and double langmuir probes, *Fusion Sci. Technol.* 75 (4) (2019) 324–329, <https://doi.org/10.1080/15361055.2019.1579623>.
- [16] S.-Y. Yoon, H. Jeon, C. Yi, S. Park, S. Ryu, S.B. Kim, Mutual interaction between plasma characteristics and liquid properties in AC-driven pin-to-liquid discharge, *Sci. Rep.* 8 (1) (2018) 12037, <https://doi.org/10.1038/s41598-018-30540-4>.
- [17] S. Gershman, A. Belkind, Electrical discharge in gas bubbles in gel, *J. Appl. Phys.* 128 (13) (2020), 133302, <https://doi.org/10.1063/5.0016273>.
- [18] E. Corella Puertas, A. Dzafic, S. Coulombe, Investigation of the electrode erosion in pin-to-liquid discharges and its influence on reactive oxygen and nitrogen species in plasma-activated water, *Plasma Chem. Plasma Process.* 40 (1) (2020) 145–167, <https://doi.org/10.1007/s11090-019-10036-3>.
- [19] S. Basnet, R.R. Pokhrel, R. Khanal, Characteristics of magnetized dusty plasma sheath with two ion species and  $q$ -nonextensive electrons, *IEEE T. Plasma Sci.* 49 (4) (2021) 1268–1277, <https://doi.org/10.1109/TPS.2021.3066888>.
- [20] Y. Han, Y. Liu, F. Lin, Z. Li, Q. Luo, Experimental investigation of arc formation and bubble expansion initiated by pulse discharge in water, in: 2015 IEEE Pulsed Power Conference (PPC), IEEE Explore, 2015, pp. 1–5, <https://doi.org/10.1109/PPC.2015.7296930>, <https://ieeexplore.ieee.org/document/7296930>.
- [21] M. Anwar, T.E. Saraswati, A. Bahrudin, Submerged electrical arc discharge for nanoparticles fabrication using carbon-based electrodes, *Mater. Sci. Forum* 939 (2018) 141–146, <https://doi.org/10.4028/www.scientific.net/MSF.939.141>.
- [22] L. Anjarwati, M. Anwar, Y. Mahardhika, R. Fadhillah, C.H.B. Apribowo, T. E. Saraswati, Y., Ayub, current-voltage monitoring of plasma arc discharge submerged in water for nanoparticles fabrication, *AIP Conf. Proc.* 2217 (1) (2020) 030185-1–030185-5, <https://doi.org/10.1063/5.0000978>.
- [23] A. Farhadi, Y. Zhu, L. Gu, W. Zhao, Influence of electrode shape and size on electric arc channel and crater, *Proc. CIRP* 68 (2018) 215–220, <https://doi.org/10.1016/j.procir.2017.12.051>.
- [24] N. Sano, H. Wang, I. Alexandrou, M. Chhowalla, K. Teo, G. Amaralunga, K. Iimura, Properties of carbon onions produced by an arc discharge in water, *J. Appl. Phys.* 92 (5) (2002) 2783–2788, <https://doi.org/10.1063/1.1498884>.
- [25] A. Traidia, F. Roger, A. Chidley, J. Schroeder, T. Marlaud, Effect of helium-argon mixtures on the heat transfer and fluid flow in gas tungsten arc welding, *Int. J. Mech. Aero. Ind. Mechatron. Manufac. Eng.* 5 (1) (2011) 6.
- [26] M. Schnick, U. Fuessel, J. Zschetzche, Simulation of Plasma and Shielding Gas Flows in Welding and Cutting Arcs with Ansys CFX, International Scientific Colloquium, Modelling for Material Processing, Riga, 2006.
- [27] S. Kolev, A. Bogaerts, A 2D model for a gliding arc discharge, *Plasma Sources Sci. Technol.* 24 (1) (2014), 015025, <https://doi.org/10.1088/0963-0252/24/1/015025>.
- [28] M. Keidar, I.I. Beilis, Chapter 6 - Plasma nanoscience and nanotechnology, in: M. Keidar, I.I. Beilis (Eds.), *Plasma Engineering*, Academic Press, Boston, 2013, pp. 287–357.
- [29] M. Keidar, I.I. Beilis, Modeling of atmospheric-pressure anodic carbon arc producing carbon nanotubes, *J. Appl. Phys.* 106 (10) (2009), 103304, <https://doi.org/10.1063/1.3262626>.
- [30] Atomic Spectra Database. NIST Standard Reference Database 78, National Institute of Standards and Technology, U.S. Department of Commerce, 100 Bureau Drive, Gaithersburg, 1995. <https://www.nist.gov/pml/atomic-spectra-database>.